Thermal−Electrical Character of in Situ Synthesized Polyimide-Grafted Carbon Nanofiber Composites

Michael J. Arlen,[†,‡] David Wang,[†,§] J. David Jacobs,[†,||] Ryan Justice,[†,||] Aaron Trionfi,[⊥] Julia W. P. Hsu,[⊥] Dale Schaffer,[||] Loon-Seng Tan,[†] and Richard A. Vaia*[,†]

Materials & Manufacturing Directorate, RXBN, Air Force Research Laboratory, Wright-Patterson Air Force Base, Ohio 45433-7750, Department of Polymers Science and Engineering, University of Akron, Akron, Ohio 44325-3909, University of Dayton Research Institute, Dayton, Ohio 45469-0168, School of Engineering, University of Cincinnati, Cincinnati, Ohio 45221, and Center for Integrated Nanotechnologies, Sandia National Laboratory, Albuquerque, New Mexico 87185

Received July 8, 2008; Revised Manuscript Received August 21, 2008

ABSTRACT: Notwithstanding the success of polymer−carbon nanotube (CNT) nanocomposites, a solid understanding of the impact of external perturbations, including temperature and stress, on the electrical response, its reproducibility, and the subsequent relationship to the topology of the percolative morphology and molecular details of the CNT−CNT contact junction is not complete. Using an in situ synthesis approach, two series of polymide (CP2)−carbon nanofiber (CNF) composites are prepared with quantitatively (small-angle X-ray scattering) comparable CNF dispersions, but differing in the structure of the CNF−polymer interface. Amino-functionalized CNFs (FCNFs) enable direct formation of CP2 grafts onto the CNFs, whereas pristine CNFs (PCNFs) result in a relatively weak interface between the carbon nanofiber and CP2 matrix. In general, low-frequency ac impedance measurements are well described by the percolation bond model, yielding a percolation threshold below 1 vol % (0.24 and 0.68 vol % for PCNF−CP2 and FCNF−CP2, respectively). However, the design of the interface is determined to be crucial for controlling the electrical behavior in four substantial ways: magnitude of the limiting conductivity, linearity of the $I-V$ response, magnitude and direction of temperature-dependent resistivity, and reproducibility of the absolute value of the resistivity with thermal cycling. These observations are consistent with a direct CNF−CNF contact limiting transport in the PCNF−CP2 system, where the CP2 grafts onto the FCNF from a dielectric layer, limiting transport within the FCNF−CP2 system. Furthermore, the grafted CP2 chains on the FCNF reduce local polymer dewetting at the CNF surfaces when the temperature exceeds the CP2 glass transition. This appears to stabilize the structure of the percolation network and associated conductivity. The general behavior of these interfacial extremes (pristine and fully functionalized CNFs) set important bounds on the design of interface modification for CNFs when the intended use is for electrical performance at elevated temperatures or under extreme current loads.

Introduction

The increasing demand for prognostics of structural components has led to the integration of metals, ceramics, polymers, and composites thereof, into structures as reversible fuses, self-regulating heating elements, thermistors, and structural integrity sensors. Compared to inorganic materials, polymers containing conductive fillers offer increased durability, processibility, and tailorability. In general, these polymer-based composites exhibit resistivity changes due to small changes in filler morphology in response to chemical absorption,[1,2] electric potentials,[3,4] mechanical deformation,[5,6] and/or temperature.[7,8] To achieve useful electrical response for these various responsive applications, conventional filled polymers utilize relatively high loadings (>20 wt %) of classic conductive fillers, such as carbon black,[8−10] ceramics,[11] chopped carbon fibers,[12,13] graphite,[14,15] and metallic flakes.[7]

Recently, the use of high aspect ratio carbon nanotubes (CNTs), whether single-wall nanotubes (SWNTs), multiwall nanotubes (MWNTs), or nanofibers (CNFs), has demonstrated the ability to significantly lower the electrical percolation threshold (Φ_c) below 1 vol % in isotropic, filled polymer systems.[16−22] Φ_c represents the filler volume fraction where electrical properties, such as conductivity, exhibit a discontinuous change—an insulator−conductor transition. The high aspect ratio and low Φ_c combine to enable the filler volume fraction to be 2−10 times the value of Φ_c at reasonable loadings (10%), thus creating a robust percolation network with multiple contacts per filler while maintaining the processibility and physical properties of the polymer matrix.

In general, filler−filler contact resistance dominants the dc and low-frequency ac conductivity in these filled systems. Thus, in addition to the topology (orientation and dispersion) of the percolation network, changes in the average number of contacts between fillers or the local structure of the filler−filler contact have a substantial impact on the macroscopic conductivity. One major challenge facing the utilization of CNT−polymer composites is the reproducibility of the materials' electrical response with temperature—i.e., the pyroresistive character. At temperatures far from a thermal transition of the polymer matrix, the resistivity of the filled polymer uniformly changes, reflecting the thermal activation of the dominant transport mechanism. However, at a matrix transition temperature, the resistivity discontinuously changes. This abrupt change reflects the impact of an increased molecular volume (melting) or coefficient of bulk thermal expansion (glass transition) on the topology of the percolation network, as well as on the average filler−filler contact distance and the number of filler−filler contacts within the percolation network. Through a combination of these effects, both positive and negative coefficients of resistivity have been reported for filled polymers.[23−31] In many instances, the increased matrix dynamics above the softening transition of the matrix alters the matrix−filler interface as well as enhances

[†] Air Force Research Laboratory.
[‡] University of Akron.
[§] University of Dayton Research Institute.
[||] University of Cincinnati.
[⊥] Sandia National Laboratory.

10.1021/ma801525f CCC: $40.75
Published on Web 10/10/2008

creep if the material is under mechanical load. These processes lead to irreversible changes in the filler−filler connectivity. The resultant percolation network created during cooling exhibits a slightly different electrical response. Thus, the absolute value of resistance can change with each cycle, limiting usefulness to a single episode.

Therefore, understanding the effects of CNT loading and the role of the interface on the pyroresistive behavior of CNT-filled polymers is important for the design of multifunctional materials. Unfortunately, it is difficult to isolate the impact of interfacial modification on electrical transport, since changes in the polymer−CNT interface nominally have a drastic impact on the dispersion of the CNT and, thus, the nature of the percolation network. Therefore, most studies must deconvolute the effect of the interface on both the topology of, and the transport through, the CNT network. Herein, the thermal−electrical behavior of two series of polyimide (CP2)[32] containing CNFs differing in the structure of the CP2−CNF interface is discussed. Since the fabrication procedure yields *quantitatively* similar CNF dispersions and morphologies, differences in electrical performance between the systems can be attributed to the interface structure. The design of the interface is determined to be crucial for controlling the electrical behavior in four substantial ways: magnitude of the limiting conductivity, linearity of the $I-V$ response, magnitude and direction of temperature-dependent resistivity, and reproducibility of the absolute value of the resistivity with thermal cycling. Combining high thermomechanical performance of CP2[33−37] with the ability to tune electrical characteristics by blending provides opportunities for a range of aerospace applications including thermistors, EMI shielding, pressure sensors, actuators, and electrodes.[19,38]

Experimental Section

Fabrication. The preparation of films of CP2, CP2−pristine carbon nanofibers (PCNFs), and CP2−amino-grafted carbon nanofibers (FCNFs) was performed via a two-stage polymerization scheme. The details are summarized elsewhere.[39] In brief, the CNFs used were heat-treated vapor-grown multiwalled nanofibers (Applied Sciences Inc., Cedarville, OH; PR-19-HT, $\rho = 1.95$ g/cm^3, $\sigma_{DC} = 7000$ S/cm, single fiber at 99.99% carbon). For FCNF films, pristine CNFs were surface functionalized with aromatic amine groups via a Friedel−Crafts acylation reaction with 4-(3-aminophenoxy)benzoic acid at 130 °C in a poly(phosphoric acid)/P_2O_5 solution with mechanical stirring. Formally, the COOH groups react with sp^{2}C−H surface defects (originating from the hydrocarbon feedstock) to produce a ketone linkage and water as a byproduct. The combined results of thermogravimetric and elemental analyses suggested that there were 5 amine functional groups per 100 carbon atoms of the CNF.[39] Pristine CNFs or amine-functionalized CNFs (0.1, 0.3, 0.5, 1, 2, 3, 5, and 10 wt %) were then dispersed homogeneously in anhydrous *N*,*N*-dimethylacetamide (DMAc; 15 mL) by sonication with a high-intensity ultrasonic processor. Then 2,2-bis(phthalic anhydride)-1,1,1,3,3,3-hexafluoroisopropane (6FDA; 1.777 g, 4.0 mmol) was added and the resulting mixture stirred under dry nitrogen at room temperature for 15 min until all the 6FDA was dissolved. 1,3-Bis(3-aminophenoxy)benzene (BAPB; 1.169 g, 4.00 mmol) was then added to the resulting solution. The dark reaction mixture was magnetically stirred at room temperature for 24 h to afford a viscous solution containing poly(amic acid) (PAA) and PCNFs (or FCNFs). The resulting mixture was diluted with DMAc (7 mL), agitated for 1 h, sonicated, and poured into a glass dish. The DMAc was evaporated under vacuum at 50 °C for 12 h, followed by heat treatment at 100 °C for 2 h, 150 °C for 2 h, 200 °C for 2 h, and 250 °C for 1 h under dry nitrogen. The film thickness ranged from 0.1 to 0.2 mm. Specific samples are referred to by the concentration (wt %) and filler type (PCNF and FCNF) from this point forward (Table 1).

It is important to note that, in separate experiments, we observed that the processing conditions, such as the initial DMAc evaporation temperature, PAA solution viscosity, and usage of high shear mixing, impacted the measured conductivity by several orders of magnitude for films containing the same type and same amount of CNFs. These small changes in processing history appear to impact everything from the degree of CNF dispersion to the extent of polymer absorbed on the CNF surface and thus the average distance between CNF−CNF contacts to the creation of a gradient in tube orientation and concentration near the surface of the film that in the extreme case manifests in a polymer-rich skin layer on the film surface that complicates facile connection of the bulk CNF network to an external circuit. Therefore, we have scrupulously followed the same processing conditions here to ensure the repeatability of the electrical measurements.

Table 1. Summary of PCNF and FCNF System Properties

sample[a]	Φ_{CNF}[b]	M_w[c] (g/mol)	PDI[c]	CP2-*g*-PCNF concn[d] (wt %)	graft M_w	T_g (°C)	CTE (μm/m°C)
CP2	0	238 400	2.83			199	168.6
0.1PCNF	0.00069	415 600	3.29			201	162.1
0.3PCNF	0.0021	198 000	2.33			202	161.2
0.5PCNF	0.0035	198 300	3.10			201	160.9
1PCNF	0.0069	154 100	2.63			199	154.5
2PCNF	0.014	153 700	2.18			197	147.7
3PCNF	0.021	140 200	2.12			196	143
5PCNF	0.035	128 460	2.25			196	138.1
10PCNF	0.069	120 130	2.02			195	128.0
0.1FCNF	0.00069	371 300	2.94	2.2	5280	203	169.1
0.3FCNF	0.0021	238 600	2.61	5.8	4640	202	168.5
0.5FCNF	0.0035	197 400	2.59	8.5	4080	201	166.0
1FCNF	0.0069	146 200	2.63	14.4	3460	200	166.3
2FCNF	0.014	135 700	2.39	28.9	3470	197	161.4
3FCNF	0.021	119 100	2.51	29.7	2380	195	156.3
5FCNF	0.035	94 300	2.25	47.5	2280	194	146.0
10FCNF	0.069	75 000	2.30	71.0	1700	194	127.1

[a] The number indicates the concentration (wt %) of CNF and is followed by the CNF type (PCNF, unfunctionalized CNF; FCNF, amino-functionalized CNF). [b] CNF volume fraction = $\Phi_{CNF} = [\rho_{CNF}$(CNF concn (wt %))]/100. [c] "Effective molar mass" determined from size exclusion chromatography calibrated with polystyrene standards. PDI = polydispersity index. [d] Calculated from the insoluble mass fraction.

Relative estimates of the weight-average molar mass (M_w) and polydispersity (PDI) of the soluble fraction of CP2 was established by size-exclusion liquid chromatography (SEC) performed on an Agilent 110 series GPC−SEC analysis system in tetrahydrofuran (THF) at 25 °C calibrated by poly(styrene) standards (Table 1). Note that the numbers reported are the "effective polystyrene molar mass" of a polyimide chain of comparable retention time. Samples were dissolved in THF, and the insoluble mass was separated. Overall, the presence of the CNFs disrupted the condensation polymerization, resulting in a decreased M_w of the soluble portion of the CP2 matrix. An exception to this trend occurred at the lowest CNF additions (0.1 wt %). The slight decrease of the glass transition temperature for both mixtures (PCNFs and FCNFs) with increasing CNF content is consistent with the lower matrix M_w (Table 1). For the PCNF−CP2 samples, the insoluble portion agreed well with the known mass of PCNFs added to the reaction, indicating complete solubility of the matrix and removal of the CP2 from the PCNF surface. For the FCNF−CP2 samples, the insoluble mass was greater than the initial FCNF loading, indicating that the amino surface functionality participated in the condensation reaction, resulting in CP2 chains grafted onto the CNFs. The weight percentage of CP2 grafted onto the FCNFs was estimated from the insoluble weight percentage in THF minus the original FCNF content. A lower estimate of the average M_w of the CP2 grafted chains was derived by assuming all the available amine sites (5 atom % relative to the CNF carbon content) participated in the condensation reaction. This estimate indicates that the M_w of grafted CP2 decreases as the FCNF loading increases (Table 1). The additional amine groups on the FCNFs will increase the number of reactive sites and produce a stoichometric imbalance by consuming 6FDA monomer and thus lowering the matrix and graft M_w.

Thermal Analysis. Differential scanning calorimetry (DSC) measurements were performed using a TA Instruments DSC Q1000 at a scanning rate of 10 °C/min in a N_2 atmosphere. The thermal glass transition, T_g, of each sample was determined as the inflection in the DSC thermogram baseline. Thermal expansion measurements were performed on a TA Instruments TMA 2940 thermomechanical analyzer in the linear expansion and penetration modes (25−210 °C) at a heating rate of 10 °C/min. The linear coefficient of thermal expansion (CTE) decreased with filler loading for both series, as expected given $CTE_{CP2} \gg CTE_{CNF}$. Note that the CTE values reported for commercial polyimides are typically lower due to additional processing techniques applied to the films such as axial stretching or rolling.[40]

Morphology. The dispersion of CNFs in CP2 was investigated using scanning electron microscopy (SEM) and ultra-small-angle X-ray scattering (USAXS). For SEM, samples were cut from the film centers and then freeze-fractured using liquid nitrogen. The freeze-fractured surfaces were sputter-coated with 2 nm of Au to reduce charging and imaged with a Hitachi S-5200. USAXS measurements were performed at the UNICAT beam line (33ID) at the Advanced Photon Source, Argonne National Laboratory. The Bonse-Hart USAXS camera used at this facility covers the regime of 10^{-4} Å$^{-1} \leq q \leq 0.1$ Å^{-1}. The data were desmeared using routines provided by UNICAT. The incident wavelength was 1 Å.

Electrical Analysis. dc current−voltage ($I-V$) measurements were performed using an Agilent 4155 parameter analyzer in a model TTP6 Lakeshore variable-temperature probe station. For these measurements, Au electrodes were deposited via an electron beam evaporator to create a sandwich device geometry. The electrodes consisted of a 50 nm thick contact that spanned the entire bottom surface of the sample and nine 20 nm thick 1 mm × 1 mm electrodes on the top surface. Note that nonlinear $I-V$ character was observed for CP2 containing FCNFs at source voltages greater than |100 mV| (see below). Thus, the reported resistance for CP2−FCNF samples must consider the source voltage, which was constant for all impendence measurements (see below).

ac impedance measurements (10^{-2} to 1.25×10^6 Hz) were performed with a Novocontrol high-resolution Alpha-A impedance analyzer coupled with the Quatro cryosystem thermal controller on 0.1−0.2 mm thick films sandwiched between 20 mm diameter Au-coated brass disks at 25 °C. Voltage-independent impedance at room temperature was observed for all CP2−PCNF samples up to source voltages of 5 V_{rms}. For the FCNF series, voltage-dependent impedance was observed with source voltages in excess of 1.0 V_{rms} and especially for samples with CNF content near the percolation threshold. This corresponds to the aforementioned nonlinear current−voltage measurements. A 1.0 V_{rms} excitation (peak voltage of 1.414 V) for all samples was chosen to balance the signal-to-noise ratio with the linear response. The extrapolated low-frequency conductivity, $\sigma_{low\text{-}freq}$ (an estimate of the dc conductivity, σ_{dc}), was determined by an extrapolation of the real part of the complex conductivity, σ', to 0 Hz. The reported $\sigma_{low\text{-}freq}$ values represent the average of three different samples for each concentration (wt %) value.

For temperature-dependent impedance measurements (−140 to +210 °C), the electrode distance was set at 25 °C. Electrode polarization effects at low frequencies were not observed in any sample during cooling to −140 °C, indicating thermal contraction did not degrade electrode contact. TMA contact probe measurements demonstrated that the out-of-plane thermal expansion from 25 to 210 °C was less than 0.2% for all samples, indicating compressive strain due to thermal expansion was minimal upon heating. Therefore, the effect of out-of-plane changes in the sample thickness on the electrode spacing, and thus the measured temperature-dependent impedance, was assumed negligible.

For the impedance measurements, a Denton Explorer 18 cryo auto high-vacuum deposition system was used to thermally evaporate 100 nm Au layers onto both sides of the sample to improve electrical coupling to the CNF network. Conductivity variations of several orders of magnitude are possible for samples without a Au surface coating. As an example, the dc conductivity of an uncoated 5PCNF sample (~2.8×10^{-3} S/cm) varied by 2−5 times with the contact pressure of the electrodes. With a deposited Au layer, the observed value became 5×10^{-2} S/cm and was independent of small changes in the contract pressure. Also, surface preparation such as polishing to regularize the film surface and remove the presence of polymer skin layers was found to either increase or decrease the measured conductivity depending on the extent of sample removal as confirmed by SEM. If only the polymer-rich skin layer was removed, conductivity values increased. However, slightly more mechanical polishing, or polishing of samples with substantial surface-exposed CNFs, resulted in a decreased conductivity arising from disruption and removal of fibers from the film surface, as observed by SEM. Regardless of surface polishing though, when a conductive layer was deposited, a stable conductivity value was produced. A high-quality, uniform Au metallization film was confirmed by SEM.

The need for a conductive surface coating is a direct consequence of the heterogeneous, two-phase morphology of these composites. Physical contact between the electrode and sample is established through contact between the highest, rigid asperities on both surfaces. If an insufficient number of these surface asperities containing CNFs that extend into the bulk and connect to the underlying percolation network are present at the surface, macroscopic characteristics of transport via the CNF network will not be observed. Rather-low-frequency impedance will reflect electrode-limited conductivity with contributions from polymer skin layers and sample surface irregularities. Applying the metallization to the sample provides in-plane surface continuity, ensuring that all available CNFs at the surface, whether exposed from high asperities or confined within surface depressions, are connected in parallel to the source potential. This maximizes the electrical coupling to the embedded conductive network.

Results and Discussion

Morphology. Figures 1 depicts the freeze-fractured surfaces for the 5PCNF and 5FCNF films. Fiber dispersion is similar irrespective of the CNF treatment, with comparable results observed at all CNF loadings fabricated. To complement the real space local observation provided by SEM, USAXS was utilized to provide a more quantitative volume-averaged comparison of the CNF network morphology. Figures 2 illustrates the X-ray scattering intensity as a function of reciprocal space, q, for the 5 and 10 wt % composites, respectively. The scattering curves for the PCNF and FCNF films are nearly identical over 3 orders of magnitude for composites of equal filler content, confirming the SEM observations that different composites of equal filler loadings have similar initial morphologies from ~10 nm to 10 μm. Specifically, the knee around $q \approx 8 \times 10^{-3}$ Å^{-1} corresponds well to the diameter of the CNFs estimated from microscopy ($d \approx 2\pi/q \approx 785$ Å).[41,42] Furthermore, the scattering intensity above $q \approx 8 \times 10^{-3}$ Å^{-1} exhibits Porod scaling (q^{-4}), reflecting a crisp interface between the CNF and matrix on the 10 nm length scale. The q^{-2} scaling of the scattering intensity at the lowest q is consistent with prior observations and is attributed to bending and distortions in the axial direction of the tube (wormlike character) arising from numerous contacts along the length of the CNF within the network.[42]

Percolation Behavior. Figure 3 compares the dc current−voltage response at room temperature for 5PCNF and 5FCNF films. While both samples exhibit an ohmic response, i.e., linear and symmetric $I-V$ character, from −0.2 to +0.2 V, the current value for 5PCNF is 9 orders of magnitude larger than that for 5FCNF! The linear $I-V$ behavior is representative of all CP2−PCNF films above the percolation threshold. Note that, during the high current observed in PCNF samples, higher bias measurements on these samples are not possible due to polymer deformation from ohmic heating. In contrast, FCNF films exhibited symmetric, but nonlinear $I-V$ response above |1 V|

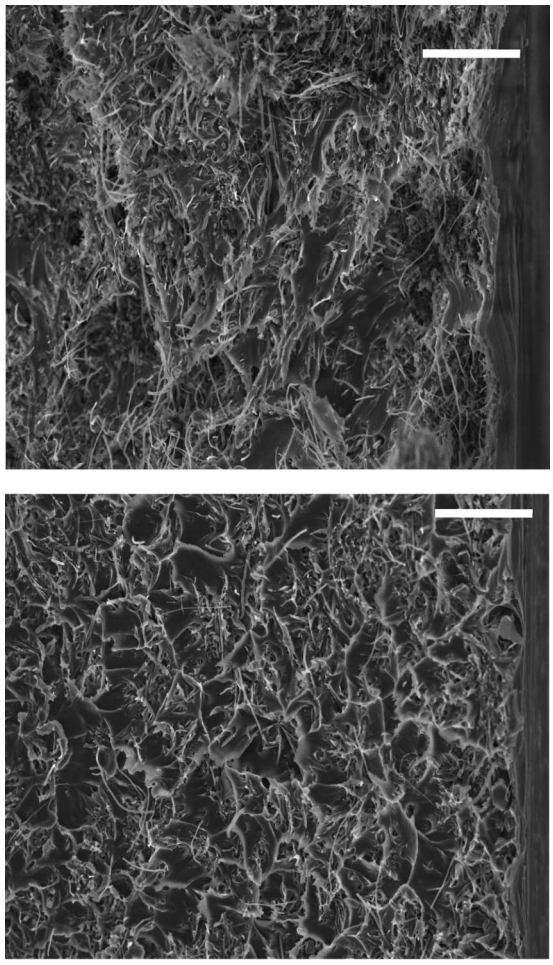

Figure 1. Scanning electron micrographs of the freeze-fractured surfaces of 5PCNF (top) and 5FCNF (bottom) systems, displaying the CNF dispersion throughout the film thickness. The scale bar is 10 μm.

at room temperature. The threshold for nonlinearity decreased with decreasing temperature, being as low as |100 mV| (from 300 to 4 K). Hence, surface modification of CNFs drastically reduces the current level and changes the transport behavior of the nanocomposites. The nonohmic character in FCNF samples implies that the mechanism limiting transport is field-dependent, such as hopping or tunneling across a narrow insulating bridge.[43] Qualitatively similar responses have been reported for discontinuous thin gold films.[43] Further examination is under way to clarify the specific mechanism underlying the nonlinearity, such as shallow-trap-limited transport, and its relation to the percolation threshold.

Figure 4 summarizes the real part of the complex conductivity, σ', at 25 °C for CP2 containing PCNFs and FCNFs. Pure CP2 and composites containing $\leq$0.3 wt % CNFs show frequency-dependent σ' behavior over the entire frequency range, where the slope of $\sim$1 indicates the CP2 and these filled systems exhibit dielectric or insulating behavior.[44] A significant change in the frequency behavior of σ' occurs when the filler loading exceeds 0.5 wt %. At low frequencies, σ' is frequency-independent up to a characteristic crossover frequency (ω_c), at which point σ' increases with frequency. At greater CNF loading, σ' is frequency-independent over the measured frequency range. These characteristics are reflective of a concentration-dependent insulator−conductor transition and parallel previous reports for other polymer-filled systems containing various forms of carbon filler.[16−18,44−48]

Figure 5 summarizes $\sigma_{low\text{-}freq}$ as a function of the volume fraction, Φ, of CNF for both systems, as well as the respective fits to the percolation bond model, where, for $\Phi > \Phi_c$, $\sigma_{low\text{-}freq} = \sigma_o(\Phi - \Phi_c)^t$ (Φ_c is the filler volume fraction at the electrical percolation threshold, σ_o is the conductivity scale factor, and t is a power law (critical conductivity) exponent).

The percolation threshold was 0.0024 and 0.0068 for the PCNF−CP2 and FCNF−CP2 systems, respectively. The Φ_c values agree with simulated values for Φ_c using electrically conductive fillers with aspect ratios greater than 100 and with SEM results confirming that the CNFs have aspect ratios of approximately 100−200.[49,50] The slightly higher Φ_c for FCNF−CP2 is consistent with an effectively lower aspect ratio arising from the surface-bound CP2 layer.[51] A 2−5 nm surface graft will increase the diameter and decrease the aspect ratio by only 5−15%. Alternatively, this may reflect slight attrition of the aspect ratio of FCNFs due to the requisite additional processing or an unquantified difference in the macroscale morphology ($>2\pi/q_{min} \approx 6$ μm). Also, the experimental error and the uncertainty in uniquely defining Φ_c from a data set spanning $\Delta\Phi \approx 10\Phi_c$ must not be overlooked. Irrespective of these differences, the Φ_c values for both systems are larger than some previous results for SWNT- and MWNT-filled polyimides.[17,20] The smaller tube diameters (SWNTs,1−2 nm;[17] MWNTs, 20 nm[20]) relative to those of CNFs (50−100 nm) result in higher aspect ratios and are consistent with theoretical simulation demonstrating that Φ_c and the filler aspect ratio are inversely proportional.[49]

The conductivity scale factor, σ_o, is proportional to the limiting conductivity of the system. In this case, it reflects the filler−filler contacts spanning through the percolation network. σ_o for the PCNF−CP2P and FCNF−CP2 systems was 1000 and 1 S/cm, respectively. The conductivity of CNF mats and estimates for individual CNFs are $\sim$7000 S/cm as reported by the manufacturer. The proximity of σ_o of the PCNF−CP2 system to the values for neat CNFs indicates that the electrical contact between CNFs within the percolation network structure is comparable to that within neat mats of CNFs. This is consistent with the linear $I-V$ character (Figure 3). The substantially lower σ_o ($\times 10^{-3}$) for FCNF−CP2 is consistent with the grafted CP2 chains acting as a thin dielectric between CNF−CNF contacts, effectively raising the contact resistance. This interfacial barrier at the junctions throughout the percolation network is also thought to be responsible for the nonlinear $I-V$ behavior. Comparable conclusions can be drawn from data presented in prior papers, such as those of Jiang[19] and Ounaies,[16] who reported $\sigma_o \leq 1$ S/cm for polyimide−carbon nanotube systems where good adhesion between the matrix and carbon nanotube was demonstrated by SEM observations of polyimide adhesion to individual carbon nanotubes. Other studies have attributed low σ_o in covalently modified CNTs to disruption of the $\pi-\pi$ bonds on the CNT surface and thus disruption of the axial conductivity of the CNTs. For example, Kim et al. attributed decreased electrical conductivity to the formation of carboxylic acid groups on multiwall carbon nanotubes (MWNTs) by H_2SO_4/HNO_3 oxidation treatment.[52] Herein though, the CNF surface functionalization process utilizes C−H defects that are susceptible to electrophilic substitution reactions (specifically, Friedel−Crafts acylation) and thus does not result in a bridge across the graphene $\pi-\pi$ structure. Thus, the observations generally imply that the relative difference in σ_o between PCNF and FCNF systems arises from the extent of the dielectric barrier between the CNF−CNF contacts within the percolation network.

Finally, the power law values of $t = 3.1$ and $t = 3.2$ for the PCNF−CP2 and FCNF−CP2 systems, respectively, are in agreement with the predicted mean field theory value of 3,[53−55] which describes heterogeneous blends of insulating and conducting phases as an effective homogeneous medium. Note that mean field behavior is not equivalent to rule-of-mixtures

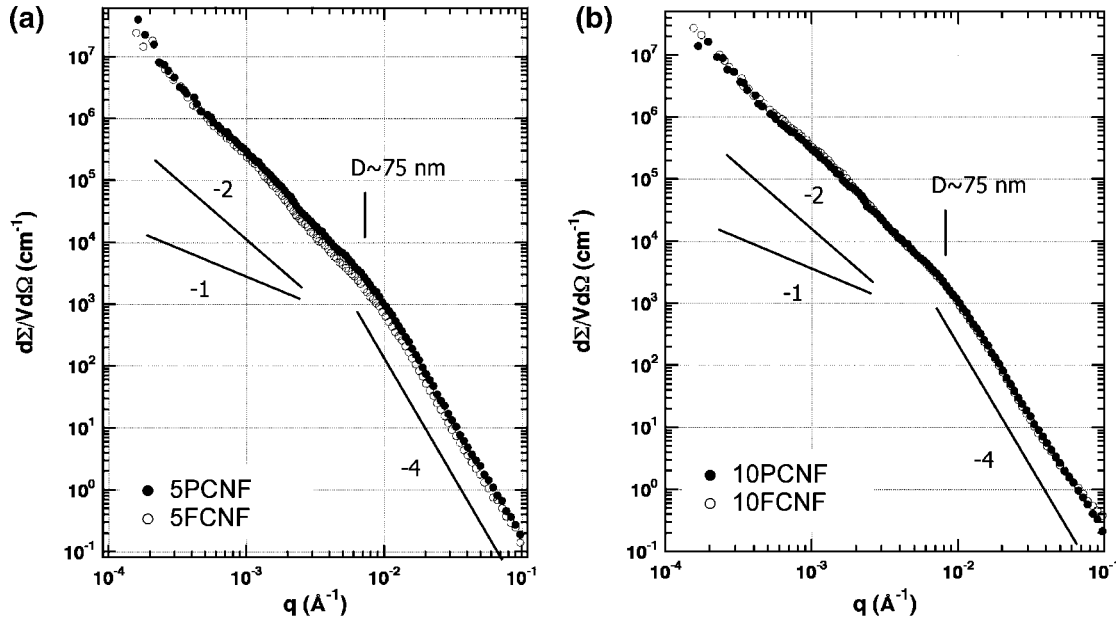

Figure 2. X-ray scattering intensity as a function of the reciprocal space, q, for CP2 containing (a) 5 wt % and (b) 10 wt % (●) PCNFs and (○) FCNFs. The scattering intensity is comparable over the observed reciprocal space range, reflecting quantitatively similar CNF dispersions for both CNF interfaces.

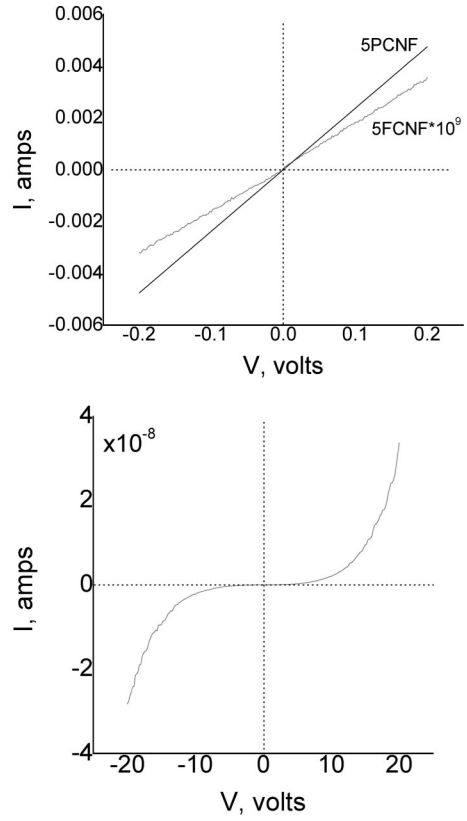

Figure 3. (Top) Current−voltage responses at room temperature for 5PCNF (black) and 5FCNF (red) films from −200 to +200 mV. 5PCNF exhibits an ohmic character, with linear and symmetric $I-V$ response from −0.2 to +0.2 V (0.15 mm thickness). Measurement to higher voltages was restricted by the current limit of the measurement instrument. In contrast, 5FCNF films exhibited symmetric, but nonlinear $I-V$ response at higher source voltages (bottom). Note that 5PCNF is much more conducting than 5FCNF and the current for 5FCNF in the figure is multiplied by a factor of 10^9.

behavior.[53−55] This is in clear disagreement with the theoretical value of $t = 2$ for the universal conductivity near the percolation threshold on three-dimensional lattices.[56] The universal behavior arises from a random number of filler−filler contacts per particle due to the random arrangement of particles on the lattice (or within the insulating medium). The resultant random number of electrical pathways implies that the environment of each transport path is also random. These concepts apply to concentrations near the percolation threshold and within the so-called "critical region" ($\Phi - \Phi_c \ll 1$), where fluctuations extend over distances that are much larger than the characteristic size of the constituents.[53] However, the quantitative definition of the critical region depends on the lattice and particle type.[54] As the aspect ratio of the filler increases (e.g., >50) and the percolation threshold decreases (e.g., <0.01), materials with filler concentrations that span the critical region into the effective medium range are accessible. In other words, samples containing volume fractions of the second phase that are an order of magnitude greater than Φ_c are available. Here the average number of contacts per particle can greatly exceed 2. Numerous others have observed $t > 2$ in various disordered insulator/conductor systems[53,57−62] In addition to topology considerations, this nonuniversality has been interpreted as a fundamental difference between lattice and continuum percolation, where the latter may exhibit nonrandom contacts between particles associated with local orientational coupling of anisotropic units and distance-dependent transport at the connections.[57−62] For example, nonuniversal behavior of $t > 2$ in three dimensions has been demonstrated for a quantum tunneling conduction model between the conductive elements in a composite[62] and for anomalous diverging distributions of conductive elements.[60] Heaney reported nonuniversal transport exponents of $t = 2.9 \pm 0.1$ in a carbon black (CB)−high-density polyethylene composite.[61] Grimaldi et al. compiled and analyzed critical exponents for various types of conductive fillers and demonstrated that nonuniversal scaling increases as the aspect ratio of the filler increases.[53]

Temperature-Dependent Resistivity. The pyroresistive behavior of filled polymer systems containing classic fillers has been investigated by many researchers.[23−31] Two general effects compete to determine the temperature dependence of the transport across the percolative network. Thermal activation of shallow trap states and diffusive transport, such as hopping, will decrease resistivity with increased temperature. In concert, the

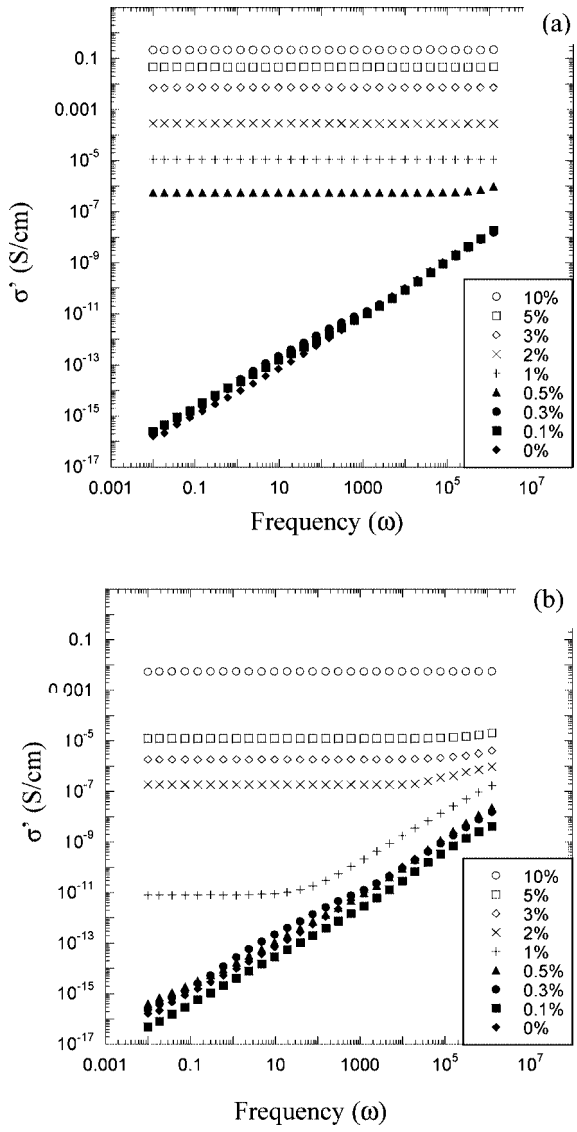

Figure 4. Real component, σ', of the complex conductivity as a function of frequency for the (a) PCNF−CP2 and (b) FCNF−CP2 series at room temperature with 1.0 V_{rms} excitation.

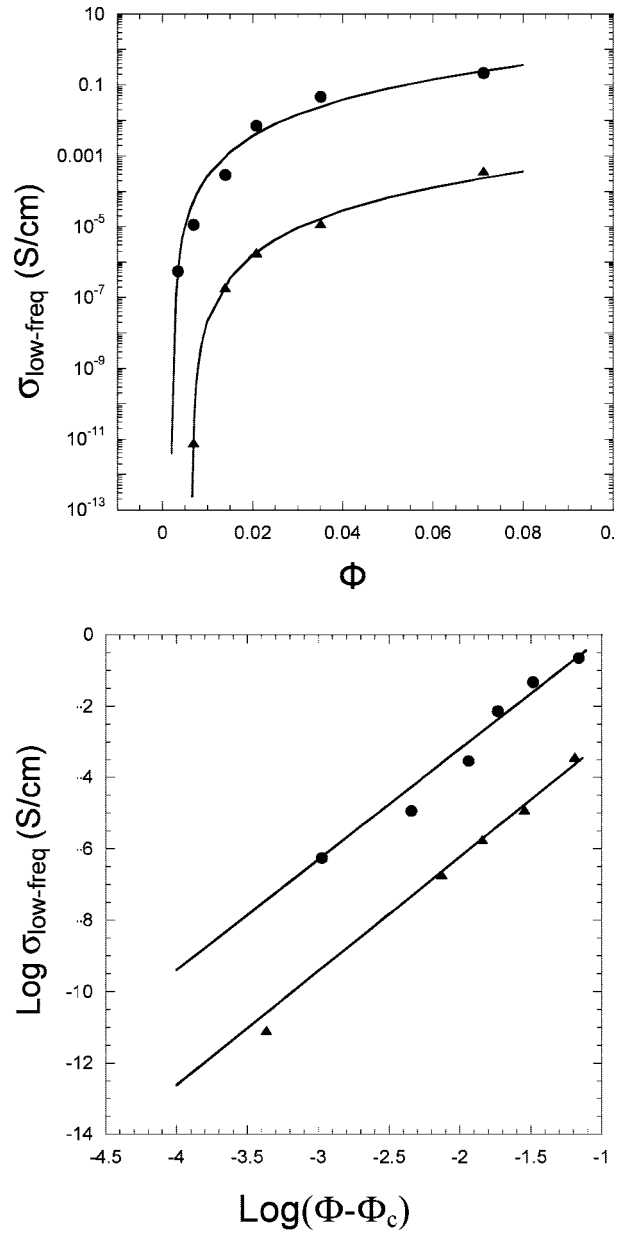

Figure 5. (Top) Extrapolated low-frequency conductivity, $\sigma_{low\text{-}freq}$ (an estimate of the dc conductivity, σ_{dc}), as a function of PCNF (●) and FCNF (▲) volume fraction, Φ. (Bottom) Linear least-squares fit of the data by the percolation bond model ($\sigma_{low\text{-}freq} = \sigma_o(\Phi - \Phi_c)^t$, for $\Phi > \Phi_c$, where Φ_c is the volume fraction at the percolation threshold). The fit parameters (Φ_c, σ_o, t) are discussed in the text. The solid lines portray the correlation between the resultant percolation bond model and $\sigma_{low\text{-}freq}$ for PCNFs and FCNFs.

contrast between bulk volume expansion of the polymer and the filler ($CTE_{polymer} \gg CTE_{CNF}$) implies that the separation between conductive filler particles increases with increased temperature and thus increases resistivity. Depending on the temperature dependence of these competing processes, two effects are observed in electrically conductive polymer composites: positive (PTC) and negative (NTC) temperature coefficients of resistivity. Increased matrix dynamics occurring above crystallite melting and glass transition temperatures substantially increases bulk volume expansion and matrix diffusivity. The subsequent increase of filler separation or matrix conductivity amplifies the PTC and NTC at these phase transition temperatures. Overall, these effects are reported in one of three ways: (i) the temperature at which the PTC or NTC substantially increases (nominally related to a matrix transition), (ii) the magnitude of the resistivity change, $\kappa(T) = R(T)/R_o$, or (iii) the thermal sensitivity, $\alpha = d\kappa/dT$, where R_o is the dc resistance at a reference temperature, T_o, and $R(T)$ is the dc resistance at temperature T.

Figure 6 summarizes representative κ, normalized to $T_o = 0$ °C, for the PCNF and FCNF systems above Φ_c. For both CNFs, the sensitivity (slope of κ) transitions from positive (PTC) to negative (NTC) with increased loading of CNFs. Also for a specific composite, the absolute magnitude of κ and α increases around the glass transition temperature (~200 °C). For example, the PTC behavior of 1PCNF mimics well the temperature dependence of the CTE for CP2 (not shown). As common for amorphous polymers, the CTE exhibits an abrupt increase around the polymer glass transition, $T_g \approx 200$ °C.

The transition from PTC to NTC behavior with increased filler loading has been previously reported and is qualitatively attributed to the density of the percolation network; for example, Quadrat et al. reported PTC to NTC transition with increased loading of short carbon fibers in polyester resins.[63] Figure 7 summarizes the thermal sensitivity, α, below and above the glass transition temperature for FCNF−CP2 composites. As previously mentioned, the absolute magnitude of the response is greater around T_g. Also, the general behavior with CNF loading

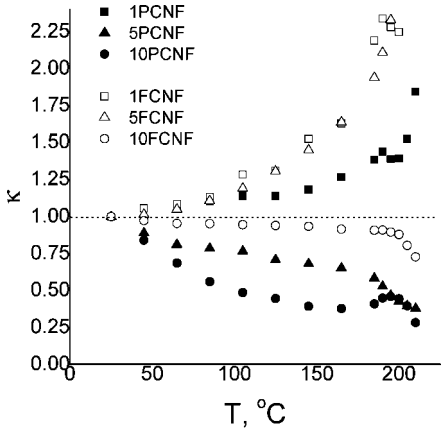

Figure 6. Normalized resistivity change, $\kappa(T) = R(T)/R_o$, as a function of temperature, T, for the PCNF−CP2 and FCNF−CP2 systems: (●) 1PCNF, (■) 5PCNF, (◆) 10PCNF, (○) 1FCNF, (□) 5FCNF, (◇) 10FCNF. Note that the reference temperature, T_o, is 0 °C and that $R(T)$ and R_o (resistance at T_o) are the low-frequency extrapolated resistances (estimate of dc resistances).

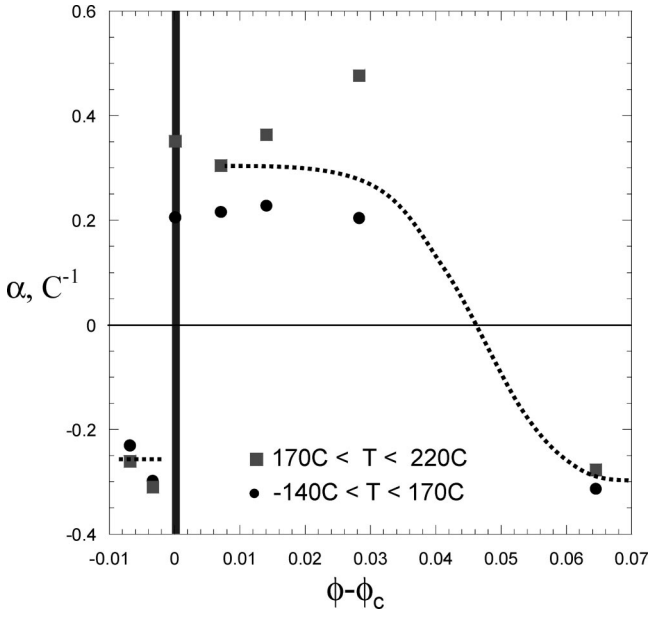

Figure 7. Thermal sensitivity, $\alpha = d\kappa/dT$, as a function of FCNF volume fraction across two temperature ranges: below (●, −140 °C < T < +170 °C) and around (■, 170 °C < T < 220 °C) T_g. Note that κ is the normalized resistivity change (T_o = 0 °C) and $\Phi_c = 0.0068$. The dotted line is a guide to the eye.

is similar above and below the glass transition temperature, indicating that the source of this behavior is associated with the impact of the CNF volume fraction on the topology of the percolation network, rather than specific temperature-dependent activation of carriers. To systematically consider the impact of CNF loading, first consider pristine CP2. CP2 exhibits an NTC, reflecting thermal activation of carriers and a decreasing resistivity with increasing temperature. This is characteristic of polymer dielectrics.[44] At the percolation threshold though, the CNFs dominate transport relative to the matrix and the bulk resistivity exhibits a PTC, reflecting the fragility of the CNF network to local disruptions in CNF−CNF contact due to matrix thermal expansion. However, at the highest loading (10 wt %), the density of contacts increases, creating a more robust network that is less sensitive to the disruption of a few contacts via thermal expansion of the matrix. Subsequently, transport is dominated again by thermal activation of carriers through the

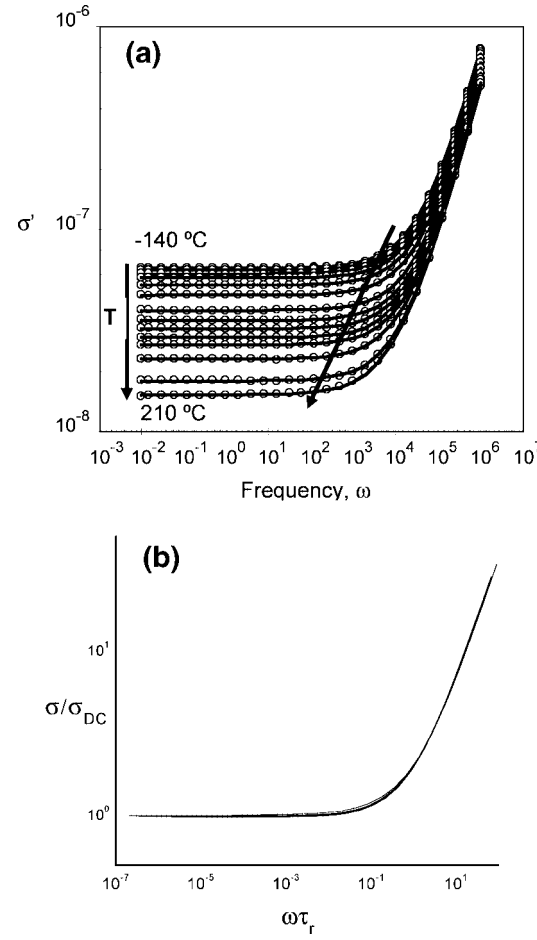

Figure 8. (a) Temperature dependence (−140 to +210 °C) of the real component of the ac conductivity, σ', for 2FCNF. (b) Subsequent master curve resulting from time−temperature superposition of σ', reflecting a normalized ac universality of the conduction process across the percolation network. Note ω is the angular frequency, σ_{dc} is the low-frequency extrapolated conductivity, and τ_r is the relaxation time defined by the universal ac conductivity model.

CNF network, exhibiting an NTC. For the CNF composites, the PTC−NTC transition occurs at a filler loading approximately 5 times that at the percolation threshold. From geometric percolation theory, the number of contacts per particle scales approximately with the product of the aspect ratio and volume fraction.[50] Thus, around 3−8 wt % CNF, the average number of contacts per CNF is between 3 and 5, reinforcing the supposition that, at these loadings, there are many connections per particle, creating a dense percolation network.

Additional evidence with regard to percolation network strengthening with increased loading of the CNF is provided by the time−temperature superposition of the impedance. As an example for FCNF composites with PTC, Figure 8 displays the temperature-dependent impendence for 2FCNF and the subsequent master curve resulting from time−temperature superposition. The impedance data are well described by the universal ac conductivity model,[44,64] in which the dispersion of the real part of the complex conductivity, $\sigma'(\omega)$, is expressed as

$$\sigma'(\omega) = \sigma_{dc}[1 + (\omega\tau_r)^n] \; (0 \le n \le 1)$$

where ω is the angular frequency, τ_r is the relaxation time, and n is the exponential dependence of conductivity at high frequency. Note that the critical frequency, given by $\omega = 1/\tau_r$, marks the frequency above which local ac transport mechanisms dominate the "in-phase" response of the complex conductivity (i.e., $\sigma'(\omega)$). In this sense, τ_r and ω_c are phenomenological model

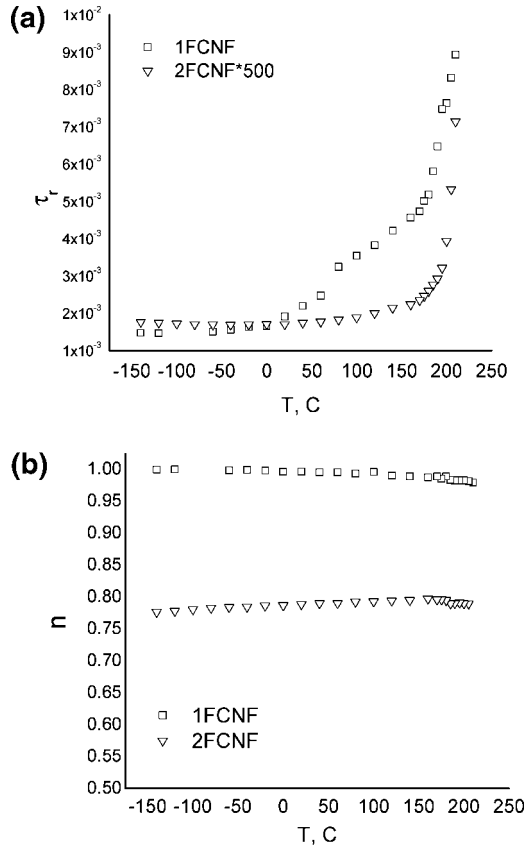

Figure 9. (a) Relaxation time, τ_r, and (b) power law exponent, n, associated with fits of the real component of the complex conductivity, σ', to the universal ac conductivity model for 1FCNF (□) and 2FCNF (▽). Due to the higher conductivity and less frequency dispersion, the relaxation time for 2FCNF is multiplied by a factor of 10^3 to compare qualitatively with that of 1FCNF. Recall that the conductivity decreases with increasing temperature, resulting in an effective negative activation energy associated with τ_r.

parameters and are not directly associated with any particular relaxation mechanism. For each temperature (−140 to +210 °C), the real component of the conductivity was normalized by $\sigma_{low\text{-}freq}$ ($\sigma_{low\text{-}freq} \approx \sigma_{dc}$) and shifted with regard to the critical crossover frequency, $1/\tau_r$, given by the least-squares fit to the universal ac conductivity model. The degree to which time−temperature superposition holds for the FCNF composites succinctly conveys the intimate relationship between long-range, low-frequency conductivity and short-range, charge transport processes.

Figure 9 compares the relaxation time, τ_r, and exponent n for 1FCNF and 2FCNF. As the temperature increases, τ_r shifts to longer times and smaller frequencies. Recall that the conductivity decreases with increasing temperature, resulting in an effective negative activation energy associated with τ_r. Qualitatively, the temperature dependence of τ_r mimics that of the matrix thermal expansion, especially for 2FCNF, which increases abruptly at $T \approx T_g$. For 1FCNF, τ_r begins to increase at temperatures much lower than T_g, consistent with a more fragile percolation network at CNF loadings near Φ_c. The very low molar mass of the surface-tethered chains could contribute to a broad distribution of local matrix relaxation events and manifest in the apparent transition around 75−100 °C; however, given the lower M_w of the 2FCNF system, it could be argued that this effect should also be apparent at higher CNF loadings. The power exponent of the frequency dependence, n, remains nearly constant for both FCNFs. The magnitude is consistent with theoretical arguments and prior experimental observations of disordered carbon-filled systems, $n \approx 0.75-1$.[48,64−66] From the theoretical constructs, n is related to the dispersion of the

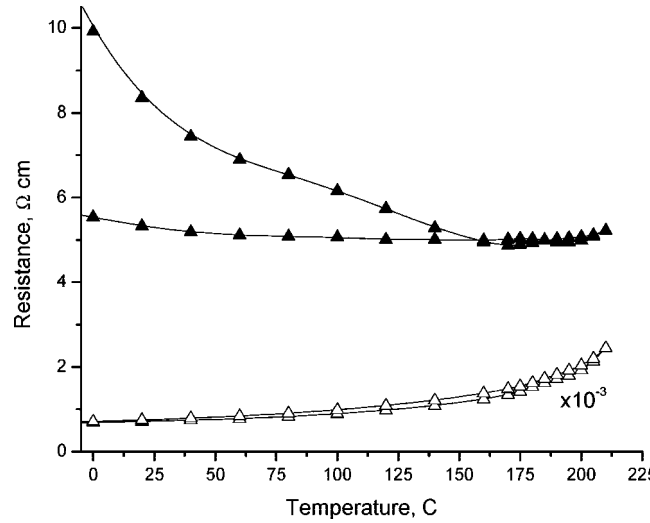

Figure 10. Temperature and thermal history dependence of the resistance ($\sigma_{low\text{-}freq}^{-1}$) for 5PCNF (▲) and 5FCNF (Δ) systems during the second thermal cycle (0 to 210 to 0 °C) after film preparation. Since 5FCNF exhibits higher resistance, the resistance values are multiplied by a factor of 10^{-3} to enable qualitative comparison. The lines through the data provide guides to the eye.

carrier mobility, where $n = 1$ is for an ideal process and is reflective of transport via a single mechanism across the network within the critical region ($\Phi - \Phi_c \ll 1$). The decrease of n as $\Phi - \Phi_c$ increases is consistent with a multiplication of paths and processes for transport through the network.

Although the detail of the polymer−CNF interface does not substantially impact the character of the concentration-dependent PTC−NTC transition, it has a substantial effect on the reproducibility of electrical characteristics during thermal cycling. Figure 10 compares the change in the resistivity of 5PCNF and 5FCNF during a thermal cycle (0 to 210 to 0 °C). For 5FCNF, the resistivity value was highly reproducible after the initial thermal cycle. For six heating−cooling cycles, the temperature dependence of the resistivity was identical to that shown. The deviation of the first heating (not shown) is attributed to thermally induced relaxation of residual stresses from the solution casting process (process history effect). Similar response was observed for the 1FCNF and 10FCNF composites. In contrast, the magnitude of the resistivity was not reproducible upon repeated thermal cycling for the 5PCNF composite. The different resistivity upon cooling relative to heating could be attributed to a structural rearrangement (or creep) of the CNF network at temperatures near and above T_g. For the PCNF system, the CP2−CNF interface is dominated by secondary interactions. It is not unreasonable to assume the interfacial stability between the heterogeneous surface of the CNF and the fluorinated polyimide will be less than if CP2 is covalently grafted to the CNF. Thus, in the melt, local dewetting of CP2 from the CNF could alter the character of the junctions throughout the percolation network. Similar conclusions have been recently drawn for CB containing thermoplastics. For example, Zhang et al. investigated CB−poly(ethylene-*co*-vinyl acetate) composites and the effect of covalently grafting poly(acrylic acid) to carbon black (FCB) on the pyroresistive response.[67] For composites containing FCB, the pyroresistive behavior was reproducible after the first thermal cycle, while the pyroresistive behavior for composites containing CB was not reproducible.

Conclusions

Polymer nanocomposites (PNCs) offer opportunities to create material systems with unique electrical, optical, and responsive

characteristics. Notwithstanding the substantial successes to date as well as some commercial products, a fundamental elucidation of the various structural factors (nanoparticle size, dispersion, interface structure, etc.) governing the properties, especially those in response to external perturbations (e.g., temperature, strain, electric field) or long-term use, are not available. Of the many reasons limiting success along these lines, including inconsistent source materials and extreme sensitivity to process history, the ability to separate morphological effects (arrangement of the nanofillers) from the properties and structure of the nanoparticle−matrix interface is arguably most acute. The uniqueness of the CP2−CNF system discussed herein is the in situ synthesis of CP2 polyimide in the presence of CNFs with vast differences in surface reactivity and the creation of nanocomposites with *quantitatively* similar morphology but differing in the structure of the matrix−nanoparticle interface. This provides a unique opportunity to examine the impact of the interface on macroscopic properties without having uncertainty arising due to a qualitatively different hierarchical distribution of nanoparticles.

In general, ac impedance measurements reveal that both FCNF−CP2 and PCNF−CP2 systems exhibit percolation behavior with conductivity scaling as $\sigma = \sigma_0(\sigma'\Phi - \Phi_c)^t$ above the percolation threshold. However, the electrical characteristics of these systems differ in four substantial ways: (1) the dc conductivity of FCNF−CP2 is 3 orders of magnitude lower than that of PCNF−CP2; (2) FCNF−CP2 exhibits nonlinear $I-V$ characteristics, whereas PCNF−CP2 systems are linear; (3) for comparable loadings the conductivity of FCNF−CP2 decreased with increasing temperature, whereas that of PCNF−CP2 increased at temperatures approaching T_g (200 °C); (4) FCNF−CP2 electrical characteristics are stable to thermal cycling (0−220 °C), whereas those of PCNF−CP2 migrate and evolve.

Conceptually, these differences are all consistent with the grafted CP2 chains on the FCNF surface restricting, on-average, direct CNF−CNF contact and dominating the interactions between the CP2 and the matrix. Specifically, for the PCNF system, the surface of the CNF is either in contact with other CNFs or directly with the CP2 matrix. Thus, an ohmic CNT−CNT contact limits transport and manifests in linear $I-V$ characteristics. The relatively weak interface between CP2 and the CNF is not stable in the melt, and thus, relaxation of the matrix from this high-energy contact continually disrupts the CNF network and minimizes reproducibility (and probably long-term stability) of the absolute electrical conductivity. In contrast, for the FCNF system, the covalently tethered CP2 chains act as a thin dielectric between CNF−CNF contacts and increase the strength of the interface with the CP2 matrix via entanglements and a general reduction of interfacial energy. This thin dielectric layer is responsible for the lower overall conductivity and nonlinear $I-V$ behavior. Furthermore, the increased interfacial strength stabilizes the interface in the melt, providing greater reproducibility of electrical characteristics during thermal cycling. Furthermore, at different CNF loadings, the similarities exhibited via the PTC−NTC transition emphasize the critical impact that the existence of multiple contacts between particles has on the electrical properties.

Finally, the combination of high thermomechanical performance of CP2 with the ability to tune electrical characteristics affords the creation of novel materials for a range of aerospace applications including smart composites, EMI shielding, morphing structures, and actuator controls. For example, the broad temperature stability (∼−140 to +200 °C) and magnitude of the PTC thermal sensitivity of the FCNF systems (0.2−0.3 C^{-1}) are comparable to those of the metals used for thermistors (Ni, ∼0.62 C^{-1}, −100 to +260 °C; Pt, ∼0.38 C^{-1}, −200 to +800 °C). These CP2 systems increase the suite of potential materials and thereby afford greater flexibility to minimize thermal mismatch within organic-based smart composites. When responsive components with a coefficient of thermal expansivity substantially different from that of the matrix resin are integrated into the composite, the thermal mismatch leads to microcracking and limits long-term durability. Overall, future exploration of the impact of the molecular architecture of the grafted chain, such as molar mass and extent of branching (dendrimeric, hyperbranched, linear), on the transport characteristics, as well as the direction and magnitude of the thermal sensitivity, will refine the foundational understanding of transport processes in these nanocomposite systems and provide new materials for electrically responsive applications.

Acknowledgment. We are grateful for the assistance of M. Houtz for thermal analysis, G. Price for SEM, and S. Z. D. Cheng and E. Tuncer for insightful discussions. M.J.A. was supported by the Intelligence Community Postdoctoral Fellowship Program. Additionally funding was provided by the Air Force Office of Scientific Research and the Materials & Manufacturing Directorate, Air Force Research Laboratory. This work was performed, in part, at the Center for Integrated Nanotechnologies, a U.S. Department of Energy, Office of Basic Energy Sciences, nanoscale science research center operated jointly by Los Alamos and Sandia National Laboratories. Sandia National Laboratory is a multiprogram laboratory operated by Sandia Corp., a Lockheed-Martin company, for the U.S. Department of Energy under Contract No. DE-AC04-94AL85000.

References and Notes

(1) Lei, H.; Pitt, W. G.; McGrath, L. K.; Ho, C. K. *Sens. Actuators, B* **2004**, *101*, 122–132.
(2) Philip, B.; Abraham, J. K.; Chandrasekhar, A.; Varadan, V. K. *Smart Mater. Struct.* **2003**, *12*, 935–939.
(3) Martin, J. E.; Heaney, M. B. *Phys. Rev. B* **2000**, *62* (14), 9390–9397.
(4) Koerner, H.; Price, G.; Pearce, N. A.; Alexander, M.; Vaia, R. A. *Nat. Mater.* **2004**, *3*, 115–120.
(5) Bloor, D.; Donnelly, K.; Hands, P. J.; Laughlin, P.; Lussey, D. *J. Phys. D: Appl. Phys.* **2005**, *38*, 2851–2860.
(6) Flandin, L.; Brechet, Y.; Cavaille, J.-Y. *Compos. Sci. Technol.* **2001**, *61*, 895–901.
(7) Martin, J. E.; Anderson, R. A.; Odinek, J.; Adolf, D.; Williamson, J. *Phys. Rev. B* **2003**, *67*, 094207-1–094207-11.
(8) Heaney, M. B. *Appl. Phys. Lett.* **1996**, *69* (17), 2602–2604.
(9) McLachlan, D. S.; Heaney, M. B. *Phys. Rev. B* **1999**, *60* (18), 12746–12751.
(10) Mather, P. J.; Thomas, K. M. *J. Mater. Sci.* **1997**, *32*, 1711–1715.
(11) Stumpler, R.; Glatz-Reichenbach, J. *J. Electroceram.* **1999**, *3* (4), 329–346.
(12) Di, W.; Zhang, G. *J. Appl. Polym. Sci.* **2004**, *91*, 1222–1228.
(13) Xi, Y.; Ishikawa, H.; Bin, Y.; Matsuo, M. *Carbon* **2004**, *42*, 1699–1706.
(14) Celzard, A.; McRae, E.; Mareche, J. F.; Furdin, G.; Dufort, M.; Deleuze, C. *J. Phys. Chem. Solids* **1996**, *57* (6), 715–18.
(15) Celzard, A.; McRae, E.; Mareche, J. F.; Furdin, G.; Dufort, M.; Deleuze, C. *Phys. Rev. B* **1996**, *53* (10), 6209–6214.
(16) Ounaies, Z.; Park, C.; Wise, K. E.; Siochi, E. J.; Harrison, J. S. *Compos. Sci. Technol.* **2003**, *63*, 1637–1646.
(17) McLachlan, D. S.; Chiteme, C.; Park, C.; Wise, K. E.; Lowther, S. E.; Lillehei, P. T.; Harrison, J. S. *J. Polym. Sci., Part B: Polym. Phys.* **2005**, *43*, 3273–3287.
(18) Barrau, S.; Demont, P.; Peigney, A.; Laurent, C.; Lacabanne, C. *Macromolecules* **2003**, *36*, 5187–5194.
(19) Jiang, X.; Bin, Y.; Matsou, M. *Polymer* **2005**, *46*, 7418–7424.
(20) Sandler, J. K. W.; Kirk, J. E.; Kinloch, I. A.; Shaffer, M. S. P.; Windle, A. H. *Polymer* **2003**, *44*, 5893–5899.
(21) Koerner, H.; Liu, W.; Alexander, M.; Mirau, P.; Dowty, H.; Vaia, R. A. *Polymer* **2005**, *46*, 4405–4420.
(22) Du, F.; Scogna, R. C.; Zhou, W.; Brand, S.; Fischer, J. E.; Winey, K. I. *Macromolecules* **2004**, *37*, 9048–9055.
(23) El-Tantawy, F.; Dichovsky, N. *J. Appl. Polym. Sci.* **2004**, *91*, 2756–2770.
(24) Dafu, W.; Tiejun, Z.; Yi, X. *J. Appl. Polym. Sci.* **2000**, *77*, 53–58.
(25) Wang, W. P.; Pan, C. Y.; Wu, J. S. *J. Phys. Chem. Solids* **2005**, *66*, 1695–1700.

(26) Bar, H.; Narkis, M.; Boiteux, G. *Polym. Compos.* **2005**, *26* (1), 12–19.
(27) Tang, H.; Chen, X.; Luo, Y. *Eur. Polym. J.* **1997**, *33* (8), 1383–1386.
(28) Mironov, V. S.; Park, M.; Choe, C.; Kim, J.; Lim, S.; Ko, H. *J. Appl. Polym. Sci.* **2002**, *84*, 2040–2048.
(29) Yi, X. S.; Shen, L.; Pan, Y. *Compos. Sci. Technol.* **2001**, *61*, 949–956.
(30) Kataoka, M.; Masuko, T. *Electr. Eng. Jpn.* **2005**, *152* (2), 337–343.
(31) Park, E. S.; Jang, L. W.; Yoon, J. S. *J. Appl. Polym. Sci.* **2005**, *95*, 1122–1128.
(32) CP2 is shortened from the original acronym LARC-CP2, which originated from a NASA research program on colorless polymides (CPs) for coating applications, where optical transparency was critical: (a) St. Clair, A. K.; St. Clair, T. L.; Shevket, K. I. *Polym. Mater. Sci. Eng.* **1984**, *51*, 62. (b) Miner, G. A.; Stoakley, D. M.; St. Clair, A. K.; Gierow, P. A.; Bates, K. *Polym. Mater. Sci. Eng.* **1997**, *76*, 381–382.
(33) Yu, A.; Hu, H.; Bekyarova, E.; Itkis, M. E.; Gao, J.; Zhao, B.; Haddon, R. C. *Compos. Sci. Technol.* **2006**, *66* (9), 1190–1197.
(34) Delozier, D. M.; Tigelaar, D. M.; Watson, K. A.; Smith, J. G.; Klein, D. J.; Lillehei, P. T.; Connell, J. W. *Polymer* **2005**, *46* (8), 2506–2521.
(35) Styers-Barnett, D. J.; Ellison, S. P.; Park, C.; Wise, K. E.; Papanikolas, J. M. *J. Phys. Chem. A* **2005**, *109* (2), 289–292.
(36) Grujicic, M.; Cao, G.; Roy, W. N. *J. Mater. Sci.* **2004**, *39* (14), 4441–4449.
(37) Qu, L.; Lin, Y.; Hill, D. E.; Zhou, B.; Wang, W.; Sun, X.; Kitaygorodskiy, A.; Suarez, M.; Connell, J. W.; Allard, L. F.; Sun, Y.-P. *Macromolecules* **2004**, *37* (16), 6055–6060.
(38) Frazier, A. B.; Allen, M. G. *J. Appl. Phys.* **1993**, *73* (9), 4428–4433.
(39) Wang, D. H.; Arlen, M. J.; Baek, J.-B.; Vaia, R. A.; Tan, L.-S. *Macromolecules* **2007**, *40*, 6100–1111.
(40) Fay, C. C.; Stoakley, D. M.; St. Clair, A. *High Perform. Polym.* **1999**, *11* (1), 145–156.
(41) Justice, R. S.; Wang, D. H.; Tan, L.-S.; Schaefer, D. W. *J. Appl. Crystallogr.* **2007**, *40*, s88–s92.
(42) Schaefer, D. W.; Justice, R. S. *Macromolecules* **2007**, *40*, 8501.
(43) Gefen, Y.; Shih, W. H.; Laibowitz, R. B.; Viggiano, J. M. *Phys. Rev. Lett.* **1986**, *57*, 3097–3100.
(44) Kremer, F., Schönhals, A., Eds. *Broadband Dielectric Spectroscopy*; Springer and Sons: New York, 2002.
(45) Flandin, L.; Verdier, M.; Boutherin, B.; Brechet, Y.; Cavaille, J.-Y. *J. Polym. Sci., Part B: Polym. Phys.* **1999**, *37*, 805–814.
(46) Potchke, P.; Abdel-Goad, M.; Alig, I.; Dudkin, S.; Lellinger, D. *Polymer* **2004**, *45*, 8863–8870.
(47) Conner, M. T.; Roy, S.; Ezquerra, T. A.; Balta Calleja, F. J. *Phys. Rev. B* **1998**, *57*, 2286–2294.
(48) Jager, K.-M.; McQueen, D. H.; Tchmutin, I. A.; Ryvkina, N. G.; Kluppel, M. *J. Phys. D.: Appl. Phys.* **2001**, *34*, 2699–2707.
(49) Munson-McGee, S. H. *Phys. Rev. B* **1991**, *43* (4), 3331–3336.
(50) Garboczi, E. J.; Snyder, K. A.; Douglas, J. F.; Thorpe, M. F. *Phys. Rev. E* **1995**, *52* (1), 819–828.
(51) Zheng, X.; Forest, M. G.; Vaia, R.; Arlen, M.; Zhou, R. *Adv. Mater.* **2007**, *19*, 4038–4043.
(52) Kim, Y. J.; Mitani, T. *J. Power Sources* **2006**, *158*, 1517–1522.
(53) Vionnet-Menot, S.; Grimaldi, C.; Maeder, T.; Strässler, S.; Ryser, P. *Phys. Rev. B* **2005**, *71*, 064201.
(54) Youngs, I. J. *J. Phys. D: Appl. Phys.* **2002**, *35*, 3127–3137.
(55) Grimaldi, C.; Balberg, I. *Phys. Rev. Lett.* **2006**, *96*, 066602.
(56) Stauffer, D.; Aharony, A. *Introduction to Percolation Theory*, 2nd ed.; Taylor and Francis: Washington, DC, 1992; p 52.
(57) Carmona, F.; Mouney, C. *J. Mater. Sci.* **1992**, *27*, 1322–1328.
(58) Lee, S.-I.; Song, Y.; Noh, T. W.; Chen, X.-D.; Gaines, J. R. *Phys. Rev. B* **1996**, *34* (10), 6719–6724.
(59) Koerner, H.; Liu, W.; Alexander, M.; Mirau, P.; Dowty, H.; Vaia, R. A. *Polymer* **2005**, *46*, 4405–4420.
(60) Balberg, I. *Phys. Rev. Lett.* **1987**, *59*, 1305–1315.
(61) Heaney, M. B. *Phys. Rev. B* **1995**, *52* (17), 12477–12480.
(62) Balberg, I. *Philos. Mag. B* **1987**, *56*, 191–1003.
(63) Vilcakova, J.; Saha, P.; Kresalek, V.; Quadrat, O. *Synth. Met.* **2000**, *113*, 83–87.
(64) Dyre, J. C.; Schroder, T. B. *Rev. Mod. Phys.* **2000**, *72*, 873.
(65) Bustingorry, S. *Phys. Rev. B* **2005**, *71*, 132201.
(66) Dyre, J. C.; Schrøder, Th. B. *Phys. Status Solidi B* **2002**, *230* (1), 5–13.
(67) Hou, Y. H.; Zhang, M.Q.; Rong, M. Z. *Polym. Compos.* **2004**, *25* (3), 270–279.

MA801525F